Biointerface Research in Applied Chemistry
Open-Access Journal (ISSN: 2069-5837)

Article
Volume 14, Issue 2, 2024, 43
https://doi.org/10.33263/BRIAC142.043

Investigation of Electrical Properties of Strontium Doped Zirconium Oxide Incorporated in Poly (Lactic-Acid)

Shruthi S. [1,2], Vinayakprasanna N. Hegde [3], Bhuvan Lokesh M [1], Jothi Ramalingam Rajabathar [4], Muthusamy Karnan [5], P Mallu [1,*]

1 Department of Chemistry, Sri Jayachamarajendra College of Engineering, JSS Science and Technology University, Mysore – 570 006, India
2 Department of Chemistry, GSSS Institute of Engineering and Technology for Women, Mysuru -570 016, India
3 Department of Physics, Vidyavardhaka College of Engineering, Mysuru-570 002, Karnataka, India
4 Department of Chemistry, College of Science, King Saud University, P.O. Box. 2455, Riyadh 11451, Kingdom of Saudi Arabia
5 Grassland and Forage division, National Institute of Animal Science, Rural Development Administration, Chungcheongnam-do, Cheonan-si 31000, South Korea
* Correspondence: pmallu@sjce.ac.in (M.P.)

Scopus Author ID 57191028289
Received: 26.03.2023; Accepted: 24.06.2023; Published: 4.02.2024

Abstract: The aim is to investigate the effect of PLA@$SrZrO_3$ nanocomposite films on the electrical characteristics of particle-stabilized PLA, with the ultimate goal of advancing electronic materials. The films were fabricated through a simple casting solvent method using different concentrations of PLA@$SrZrO_3$ nanointegrates. Characterization techniques such as X-ray Diffraction (XRD) and Scanning Electron Microscopy (SEM) were employed to confirm nanoparticles' effective doping and homogeneous dispersion in the PLA polymer. Fourier Transform Infrared Spectroscopy (FTIR) was used to identify the interaction between $SrZrO_3$ and PLA, while UV-Vis spectroscopy was employed to investigate the optical properties of the synthesized nanocomposites. The XRD analysis revealed improved crystalline characteristics of the nanocomposites with increasing dopant concentration. The FTIR absorption spectra indicated similar characteristics between neat PLA and PLA@$SrZrO_3$ nanocomposites. The UV-visible absorbance of the nanocomposites increased while the transmittance decreased. Furthermore, the study found that the dielectric properties, AC conductivity, and charge dissipation increased with the addition of nanofillers and decreased with increasing frequency. These novel findings contribute to understanding the electrical behavior of PLA@SrZrO3 nanocomposites and provide valuable insights for developing electronic materials.

Keywords: $SrZrO_3$; PLA; dielectric; electrical studies; thin film

1. Introduction

Polymers with strong dielectric properties have attracted significant interest in microelectronics due to their high breakdown field strength, good flexibility, efficient security processing, low processing temperature, low cost, and lightweight characteristics [1-3]. In the continuous development of the microelectronics industry, polymers with high dielectric properties have attracted significant attention because they have a high breakdown field strength, excellent flexibility, effective security processing, low processing temperature, low cost, and lightweight [4-6]. Numerous efforts have been made to enhance the dielectric properties of polymers due to their low dielectric constant, which restricts their potential

applications [7]. One commonly employed method in developing polymer nanocomposites is utilizing fillers with exceptional dielectric properties [8]. By incorporating nanoparticles, the dielectric constant of polymers can be increased. These composite films offer cost-effectiveness, flexibility, and ease of processing, making them suitable for various modern electronic devices and electrical power systems, such as advanced electric vehicles, biomedical equipment, fixed power grids, and portable electronics [9]. The use of biopolymers such as poly(lactic acid) (PLA) for the creation of these long-lasting goods is desirable, as the volume generated by the disposal of this electronic equipment is expanding and becoming harder to manage [10]. PLA (polylactic acid) has limitations, such as poor water and oxygen barrier qualities, stiffness, low impact resistance at ambient temperature, and low melt strength. However, researchers and industry professionals have been exploring the incorporation of PLA with various nanoparticles as a means to mitigate these drawbacks. This approach has garnered significant interest from both the industrial and academic sectors due to PLA's desirable qualities, including biodegradability, biocompatibility, excellent mechanical performance, and cost-effectiveness [11]. These multifunctional advanced materials benefit from filler-specific optoelectrical characteristics and superior matrix processability for photonics and optoelectronics applications.

Inorganic nanoparticles (NPs) can be incorporated into a polymer to create high-performance new materials with improved properties. Inorganic nanoparticles stand out for their unique optical, electrical, mechanical, and thermal capabilities, including excellent stability, a large surface area, adaptable compositions, and various physicochemical multifunctionality. Research has been conducted in the field of structural polymer-based nanocomposites, but far less study has been conducted in the field of polymer nanocomposites for functional purposes [12]. Among the functional nanomaterials, nanocomposites of metal nanoparticles dispersed in a dielectric matrix are particularly interesting due to their novel properties and hosts of new applications [13]. Polymer nanocomposites are nanomaterials created by combining nanoparticles with a polymer matrix. Polymers are the combinations of monomers. Polymer nanocomposites are polymer matrix composites containing nanosized inorganic particles. Investigating the electrical properties of strontium strontium-doped zirconium oxide incorporated in Poly (lactic acid) is one example where the synergistic influence of both component materials can be observed, combining the best qualities of each component [14]. The life cycle of durable materials has decreased throughout the decades due to the development of technologies that render such equipment obsolete in shorter periods. This is true for consumer devices such as televisions, computers, and mobile phones, which have a shorter life cycle due to annual replacement with superior products [15].

The present investigation focuses on the synthesis, fabrication, and electrical properties of new and novel PLA@SrZrO3 nanocomposites obtained using the solution casting technique. The influence of $SrZrO_3$ nanoparticle addition and their varying weight fractions on PLA films' optical and structural characteristics have been analyzed by ultraviolet (UV) and Fourier transform infrared spectroscopy (FT-IR) techniques. The morphological characteristics of PLA@$SrZrO_3$ nanocomposites were analyzed by scanning electron microscopy (SEM). The electrical properties of PLA@$SrZrO_3$ nanocomposites, such as dielectric constant (ε′), were evaluated by employing LCR meter to probe the effect of $SrZrO_3$ addition on the dielectric properties of the PLA matrix.

2. Materials and Methods

Polylactic acid (PLA) (M.W.296.4g/mol), Strontium nitrate (SD fine), Zirconium (III) nitrate hexahydrate (Sigma Aldrich). All the reagents used were of analytical grade. All the chemicals were used as they were without further purification. Deionized water is used for the experiment.

2.1. Synthesis of $SrZrO_3$ nanoparticles.

In the present study, $SrZrO_3$ nanoparticles are prepared by the solution combustion method. The main advantage of the solution combustion approach for preparing nanoparticles is the short reaction time and energy savings, which is especially beneficial for preparing complex oxides. Furthermore, the solution combustion method has special benefits such as in-situ doping of oxides, well-developed porosity, and a large specific surface area resulting from gas evolution during combustion. Strontium-doped Zirconium oxide ($SrZrO_3$) was prepared using the solution combustion method. 0.02M Strontium nitrate, 0.08M Zirconium nitrate, glycine, and sucrose are dissolved in 100 ml of distilled water. This mixture is heated for 6 hours at 70°C. To obtain mixed Strontium/Zirconium nanoparticles, the product was formed in a pale-yellow color that is porous and fluffy, and it was calcined at 500°C for 1 hour in a muffle furnace.

2.2. Preparation of poly (lactic acid)@$SrZrO_3$ nanocomposite film.

Metal oxide-doped PLA films have been fabricated via the solution casting method. This method dissolves 1.5g of PLA in 20ml of chloroform. $SrZrO_3$ nanoparticle is added to 20 ml of PLA solution in various amounts to get 0.5%, 1%, 2%, and 4% (wt/wt) $SrZrO_3$ with PLA. The mixture was stirred for 2 hours, and a Petri dish was used to cast this viscous mixture. It's left to dry at room temperature. Control PLA films were made using the same procedure but without adding $SrZrO_3$. The resultant films were almost uniform in thickness, with an average thickness of around 1.2 mm.

2.3. Characterization.

The structure of the $SrZrO_3$ nanoparticles was characterized by powder X-ray diffraction (Rigaku Proto powder diffractometer equipped with monochromatic Cu kα (λ= 0.154059 nm) radiation). The structures of pure PLA and its NC films were analyzed by XRD to study the effect of NP content on the crystallinity of the PLA matrix. The morphology of pure PLA and PLA@$SrZrO_3$ nanocomposite films was studied using a Scanning Electron Microscope (SEM, Carl Zeiss, model EVO LS15). The UV-Vis spectrum was obtained using a Beckman Coulter UV-Visible spectrophotometer (model DU 730) to study the optical properties of prepared films; the spectral data was recorded from 200-800 nm at a resolution rate of 1nm. FTIR spectra were obtained to study the interactions between PLA@$SrZrO_3$ filler material using the attenuated total reflection (ATR) mode utilizing JASCO 4100 spectrometer, Japan, at 16 cm^{-1} resolution in the wave number range 400–4000 cm^{-1}.

2.4. Dielectric studies.

The dielectric properties of the prepared nanocomposite were studied in a range of temperatures (25°C to 125°C) and frequencies (50 Hz to 5 MHz). The sample films of size 2.5

x 2.5 cm^2 were considered for this study. The silver paste was applied on both sides of the films before placing between the electrodes. The computer-interfaced NF LCR meter (Model: ZM-2376, Make: Japan) was employed to study the dielectric constant (k), impedance (Z), and ac conductivity (σ_{AC}).

3. Results and Discussion

3.1. Synthesis of PLA@$SrZrO_3$ film.

The PLA films have been fabricated through the solution casting method. The PLA films were prepared by adding $SrZrO_3$ nanoparticles in various amounts. The control PLA film was prepared without the addition of $SrZrO_3$. The PLA@$SrZrO_3$ nanocomposite films were prepared by dissolving PLA in chloroform, and then the $SrZrO_3$ nanoparticle was added to PLA solution in various amounts to get $SrZrO_3$ with PLA. The mixture was stirred for 2 hours. This viscous mixture is cast on a Petri dish. It is dried at room temperature. The films obtained were uniform, with a thickness of 1.2 mm.

3.1.1. X-ray diffraction studies.

The XRD patterns of PLA and PLA@$SrZrO_3$-NCs are shown in Figure 1. A single, intense peak at 2Θ = 25.3° can be observed, along with additional 2Θ values at 30.6°, 36.5°, and 44.1°, demonstrating the remarkable crystallinity of the synthesized $SrZrO_3$ nanoparticles. In addition to the broad diffraction peak, which was centered at 16.63° and could be assigned to pure PLA, showing the PLA polymer's nature, whereas PLA@$SrZrO_3$ NCs has characteristic ~~5~~ five diffraction peaks were observed at 2θ° of 16.8°, 25.5°, 31.2°, 36.5°, and 44.3°. Their intensities and sharpness were markedly enhanced with the increasing SrZrO3 NPs content in the polymeric matrix, suggesting a significant interaction between the matrix polymer and the filler. XRD peaks of $SrZrO_3$ NPs broadenings (0.5, 1, 2, and 4 wt%) were mostly generated by the nanosized particles existing in the nanocomposites. Based on the information in Figure 1, it was also observed that the five diffraction peak intensities increased when the fraction of $SrZrO_3$ NPs in PLA increased. This implies that the $SrZrO_3$ NPs existed on the surface and inside PLA sheets.

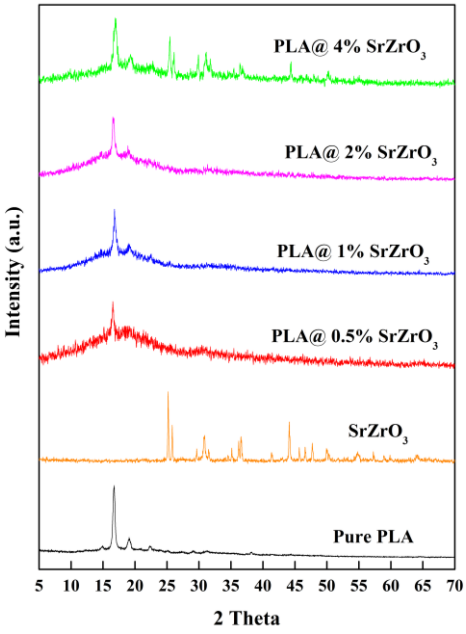

Figure 1. XRD pattern of as-synthesized $SrZrO_3$ nanoparticles, PLA, and PLA@$SrZrO_3$ nanocomposites.

3.1.2. FT-IR.

The FT-IR spectra of PLA and PLA@$SrZrO_3$ nanocomposites were collected, as shown in Figure 2. The FT-IR absorption spectra of neat PLA and PLA@$SrZrO_3$ nanocomposites are almost equivalent. In the pure PLA spectrum, the weaker peak at 2993 cm^{-1} appears due to the asymmetric stretching vibrations of $–CH_3$ and $–CH_2$. The broad absorption band at about 1740 cm^{-1} in pure PLA is caused by C=O stretching vibrations of the carbonyl group, whereas the peak at 1072 cm^{-1} is caused by C-O stretching vibrations. In PLA@$SrZrO_3$ NCs, the carbonyl (C=O) and C-O groups absorb a higher stretching frequency in the same region and shift to a higher intensity as $SrZrO_3$ content increases, this shift confirming the presence of a physical interaction between $SrZrO_3$ nanoparticles and PLA.

Further, an absorption peak at 757 cm^{-1} is consistent with Zr-O octahedron vibration modes. The residual peaks in the region of 1081-500 cm^{-1} are ascribed to bending mode, whereas the peak at 1300-1000 cm^{-1} is assigned to Zr-O-Sr bending mode, which could be attributed to the presence of $SrZrO_3$ in NCs. PLA@$SrZrO_3$ nanocomposites show almost the same absorption peaks as pristine PLA [17]. This means that no new bond formed within the nanocomposites, but upward shift intensity also suggests that strong interactions between $SrZrO_3$ and PLA exist. The physical mixing of PLA and $SrZrO_3$ caused by the addition of nanoparticles likely contributed to the constant signal at 1740 cm^{-1} and 1072 cm^{-1}. Overall, no new peaks were detected for the PLA@$SrZrO_3$ nanocomposite films, which indicated that except for the surface hydroxyl group present on the $SrZrO_3$ nanoparticles, the components were only physically mixed.

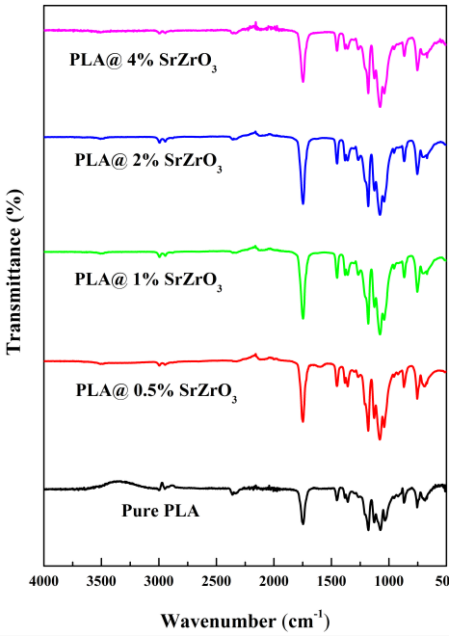

Figure 2. FT-IR spectra of PLA and PLA@$SrZrO_3$ nanocomposites.

3.1.3. FE-SEM.

Scanning electron microscope (SEM) images of pure PLA film and PLA@$SrZrO_3$ NCs film are shown in Figure 3. The sample images demonstrate their homogeneous surfaces or no observable agglomerations. It can be seen that the uniform distribution of $SrZrO_3$ nanoparticles in the PLA matrix is well-embedded with each other. The XRD spectrum is collected for 0.5, 1, 2, and 4 wt% PLA@$SrZrO_3$ NC film, as shown in Figure 1, and provides evidence for the existence of $SrZrO_3$ in the creation of nanocomposite films based on PLA@$SrZrO_3$ NC. This

result further confirms the good dispersion of $SrZrO_3$ nanoparticles in the PLA@$SrZrO_3$ NC. The strong contact and exceptional interfacial compatibility between the filler ingredient and the polymer matrix may cause this remarkable dispersion [16].

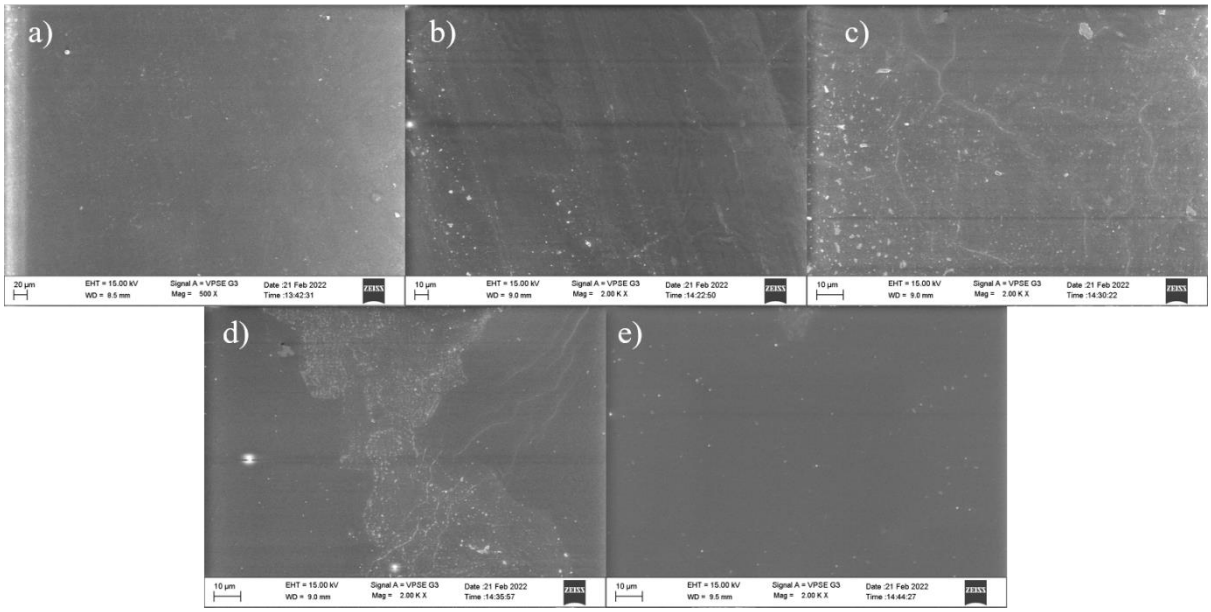

Figure 3: SEM images of Pure PLA film and PLA@$SrZrO_3$ **(a)** PLA, **(b)** 0.5% $SrZrO_3$, **(c)** 1% $SrZrO_3$, **(d)** 2% $SrZrO_3$, **(e)** 4% $SrZrO_3$.

3.1.4. UV-visible spectral studies.

UV-Vis spectroscopy was used to examine the optical properties of PLA and PLA@$SrZrO_3$ nanocomposite films. The UV-Vis absorbance and transmittance peaks of pure PLA film and PLA@$SrZrO_3$ NC films are shown in Figure 4 a-b. It has been observed in Figure 4.(a), PLA has low absorbance in the visible region. The optical absorption in the UVC (200-279 nm) range, on the other hand, is the highest. Moreover, an ideal spectral manipulator must cover the entire UV spectrum of terrestrial sunlight (UVA, UVB, and UVC). One strong absorption peak at 273 nm was observed for pure PLA. PLA has high absorption in the UV region and low absorption in the visible area. While in PLA@$SrZrO_3$ nanocomposites, all the peaks are increased in UV region. The absorbance of the film rises with an increase of $SrZrO_3$ concentration in the PLA matrix. The lower UV cut-off wavelength is around 296 nm. The optical band gap energy of the PLA@$SrZrO_3$ is calculated using the formula Eg =1240/λ (nm) in eV, where λ is the lower cut-off wavelength (296 nm). The optical band gap of the molecule is found to be 4.1 eV.

The UV–Vis transmittance spectra of pure PLA and PLA@$SrZrO_3$ nanocomposite films are shown in Figure 4b. The pure PLA film exhibited a very high transmittance in visible ranges. With the increasing $SrZrO_3$ NPs content, i.e., from 0.5 to 1%, the nanocomposite films showed a slight decrease in the transmittance in the visible range. At higher content of $SrZrO_3$ NPs (over 2%), the nanocomposite films showed a mild decrease in the transmittance to ~20% in the UV range but a dramatic decrease of ~30% in the visible range. The PLA nanocomposite films showed a considerable decrease in transmittance to ~50% in the UV spectrum with a greater concentration of $SrZrO_3$ NPs (above 4%). PLA@$SrZrO_3$ film is more transparent in the visible region.

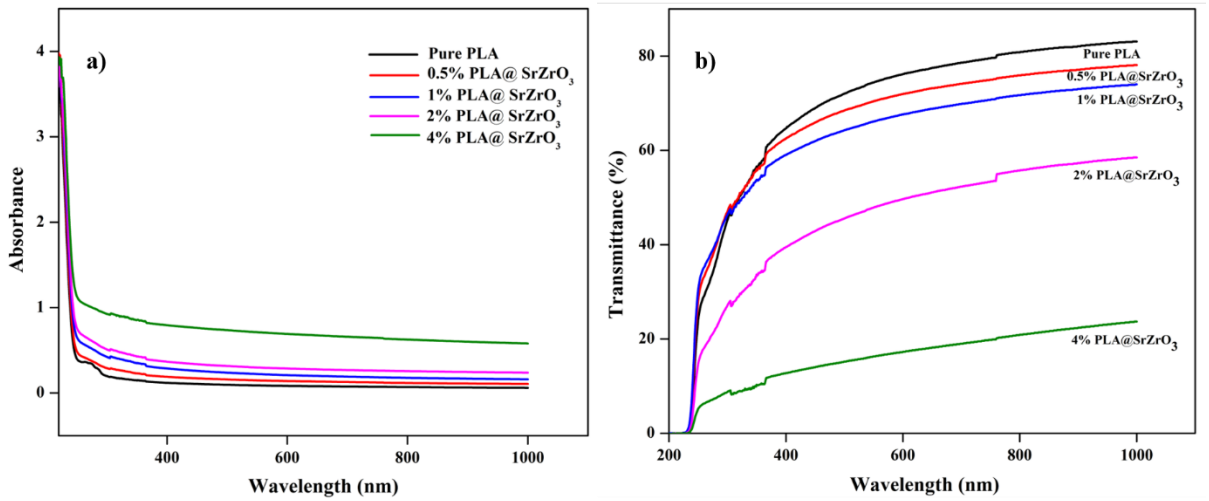

Figure 4. UV-visible **(a)** absorbance and **(b)** transmittance spectra of PLA@$SrZrO_3$ nanocomposites.

3.1.5. Dielectric constant.

The variation of the dielectric constant with frequency and temperature is shown in Figure 5. In all the figures, three trends of dielectric constant with an increase in temperature can be identified: uptrend, saturation, and downtrend. The dielectric constant increased with an increase in frequency at low low-frequency regions and decreased at higher-frequency regions. The dielectric property of systems is governed by the interfacial and orientation polarization when subjected to an AC field. The interfacial polarization originates at the interface of different groups present in the sample and the orientation polarization; the polar groups present in the nanocomposite will tend to orient themselves in the direction of AC field [17-20]. Therefore, the higher the orientation of the polar groups and interfacial polarization, the higher the dielectric constant will be. At lower frequencies, the dipoles get adequate time to orient themselves toward the AC field. But with an increase in frequency, the interfacial and orientation polarization get reduced since with the increase in frequency, the dipoles get very less time to orient in the direction of the field. In (PLA+2% & 4% $SrZrO_3$) nanocomposites, the dielectric constant decreases to negative values and increases at higher frequencies. The negative dielectric constant may be due to the reduced plasma frequency and an induction effect [21]. The increase in dielectric constant at higher frequencies in these composites may be due to a barrier inside the material caused by a built-in electric field. Therefore, the barrier capacitance may predominate in this frequency range. It can be seen that the dielectric constant is increasing with increasing temperature. This can be interpreted as the dipoles not being able to orient themselves at low temperatures. The increase in temperature helps dipoles to orient, increasing the dielectric constant [22]. The opposite behavior can be observed in (PLA+2% & 4% $SrZrO_3$) nanocomposites at a certain frequency range, and it is due to disruption in the orientation of dipoles.

The variation of the impedance with frequency and temperature is shown in Figure 6. It can be seen that the value of impedance decreases with increase in the frequency and temperature. The inset figure clearly shows the dependence of impedance on temperature. This nature of impedance suggests an increase in the AC conductivity and is confirmed by Figure 7. At low-frequency regions, the impedance decreases with a temperature rise, showing behavior similar to that of semiconductors [23]. At high-frequency regions, the impedance values merge and become independent of frequency and temperature. This is due to the release of space charges resulting from the decrease in barrier properties of the material [24].

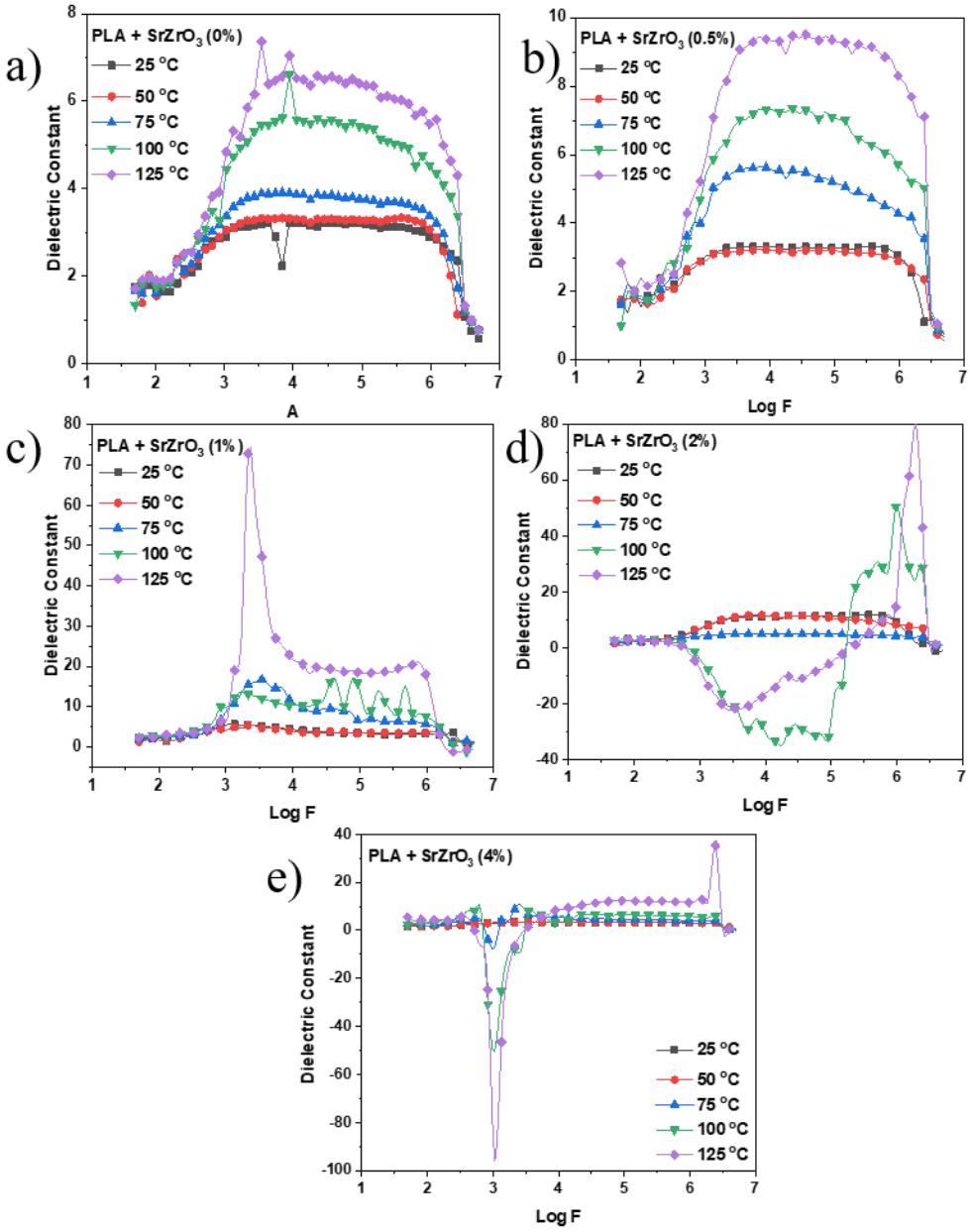

Figure 5. Dielectric constant vs. Log F for PLA@$SrZrO_3$ nanocomposites.

AC conductivity is an important parameter to understand the ionic transport properties of materials. It is determined using the following relation;

$$\sigma_{AC} = 2\pi f \varepsilon_0 \varepsilon' tan\delta \quad (1)$$

where f is the frequency of the applied field, ε' is the imaginary part of the dielectric constant and ε_0 is the permittivity of free space. The variation of the AC conductivity with frequency and temperature is shown in Figure 7. All the prepared samples exhibit the typical nature of ionic material. The conductivity is independent of frequency in the low-frequency region (DC plateau) and increases as the frequency increases. This phenomenon of conductivity dispersion is usually analyzed by Jonscher's universal power law and is given by;

$$\sigma(\omega) = \sigma_{DC} + A\omega^n \quad (2)$$

where, σ_{DC} is the dc conductivity, A is the temperature dependent factor, ω is angular frequency and n is the frequency exponent of the mobile ions. It is noted that the conductivity is independent of temperature, also at low frequencies. Hence, no variation in conductivity is observed in DC plateau. However, an increase in conductivity at higher frequencies can be observed in samples with higher dopant concertation (PLA+2% & 4% $SrZrO_3$).

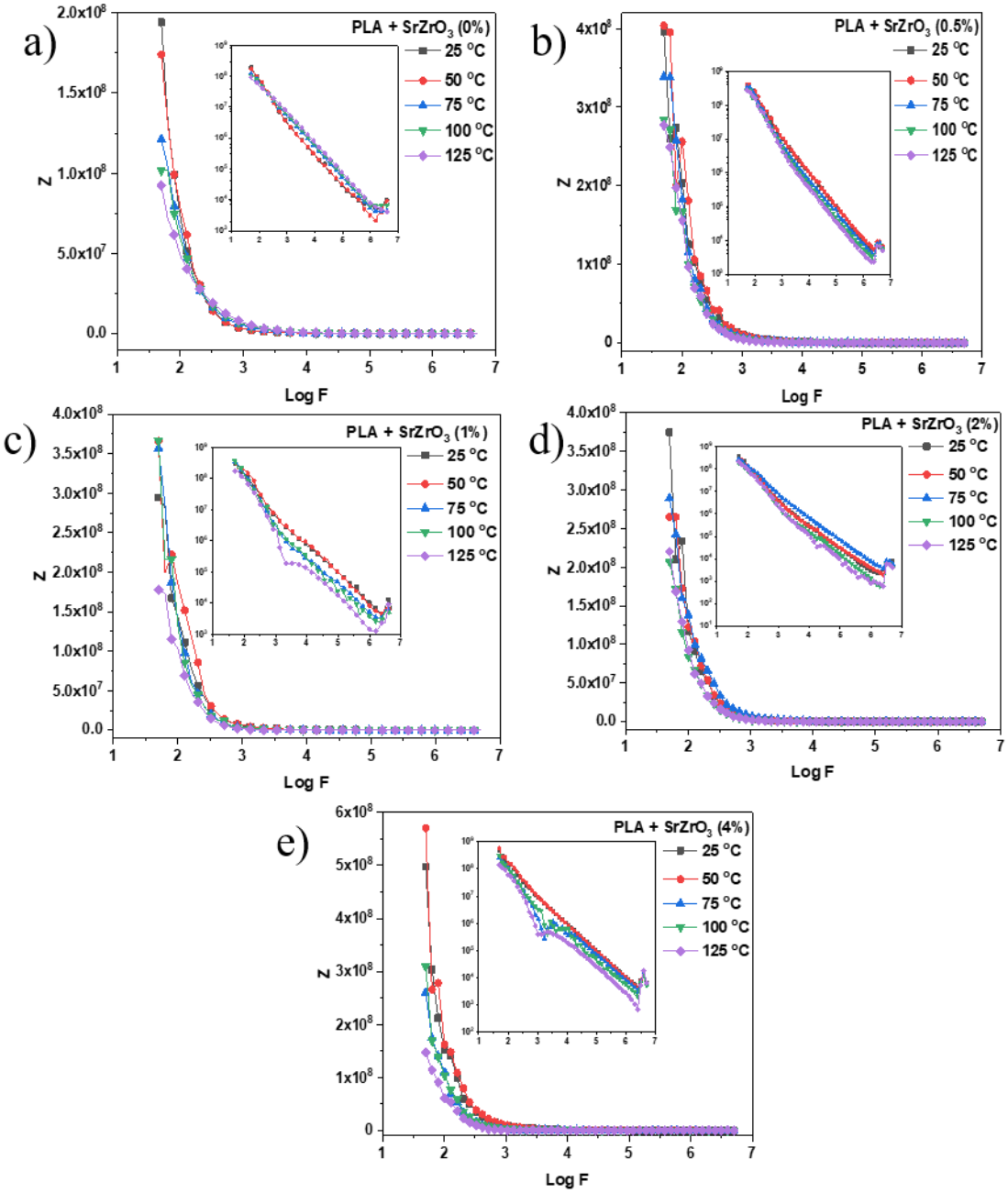

Figure 6. Impedance (Ω) vs. Log F for PLA@$SrZrO_3$ nanocomposites.

4. Conclusions

Polymer nanocomposites exhibit considerable promise for various applications due to their desirable properties. In this study, a series of PLA nanocomposites (NCs) were formed by incorporating varying concentrations (0.5, 1.0, 2.0, and 4.0 wt%) of $SrZrO_3$ nanoparticles (NPs) into the PLA matrix. These fabricated films underwent thorough characterization through techniques such as FTIR, XRD, UV, SEM, EDX, and evaluation of their dielectric properties. The incorporation of $SrZrO_3$ nanoparticles into the PLA matrix was effectively achieved, resulting in stable nanoparticle dispersions within the polymer, as evidenced by the strong bond observed between the organic polymeric host and the inorganic nanofiller in the XRD studies. The interaction between $SrZrO_3$ and PLA was also identified through FT-IR analysis using a Fourier Transform InfraRed spectrophotometer.

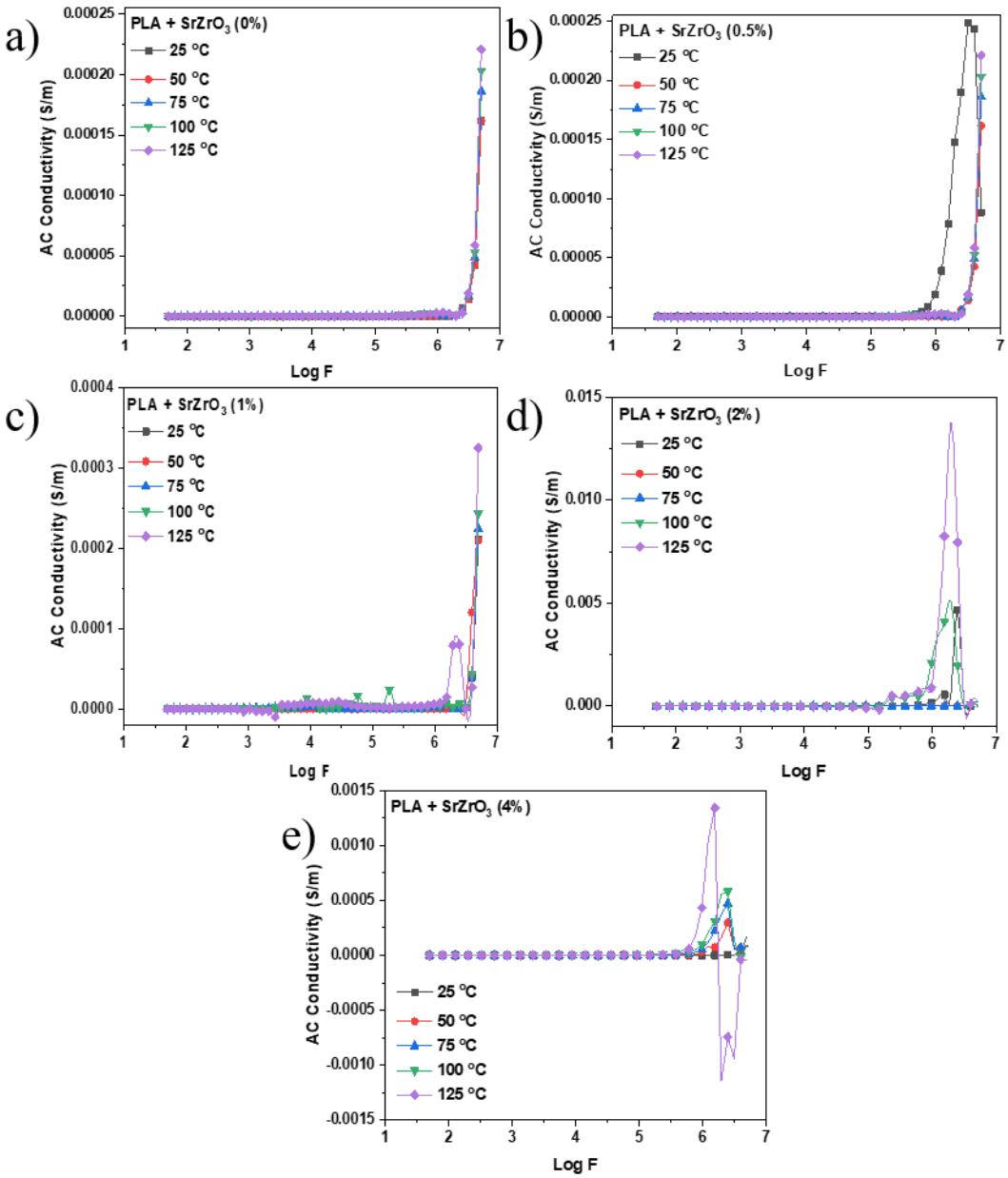

Figure 7. AC conductivity vs. Log F for PLA@$SrZrO_3$ nanocomposites.

Furthermore, the PLA@$SrZrO_3$ nanocomposites exhibited a significant increase in the UV region, coupled with satisfactory visible light transmittance. UV-visible absorption studies revealed a sharp absorption throughout the entire UV region, with absorption maxima observed at 273nm while maintaining high transparency in the visible spectrum. However, with an increase in filler loading and frequency, the AC conductivities of the fabricated films demonstrated an upward trend. These findings present a valuable method for fabricating PLA@$SrZrO_3$ nanocomposites that possess a desired combination of electrical properties specifically tailored to meet the requirements of specific device operating environments. Therefore, this study introduces a novel and straightforward approach to creating electrical materials with significant potential for various applications.

Funding

This research received no external funding.

Acknowledgments

The authors are thankful to SJCE, JSS Science and Technology University, and author (P. Mallu) acknowledges VGST - CISEE Project (GRD 647), GOK, and author (R. Jothi Ramalingam) acknowledges Researchers Supporting Project Number (RSP-20231/R354) King Saud University, Riyadh, Saudi Arabia for all support.

Conflicts of Interest

The authors declare no conflict of interest.

References

1. Yang, M.; Li, Q.; Zhang, X.; Bilotti, E.; Zhang, C.; Xu, C.; Gan, S.; Dang, Z.M. Surface Engineering of 2D dielectric polymer films for scalable production of High-Energy-Density films. *Prog. Mater. Sci.* **2022,** *128,* 100968. https://doi.org/10.1016/j.pmatsci.2022.100968.
2. Zhou, Y.; Li, L.; Han, Z.; Li, Q.; He, J.; Wang, Q. Self-Healing Polymers for Electronics and Energy Devices. *Chem. Rev.* **2023,** *123*, 558-612. https://doi.org/10.1021/acs.chemrev.2c00231
3. Feng, C.P.; Wei, F.; Sun, K.Y.; Wang, Y.; Lan, H.B.; Shang, H.J.; Ding, F.Z.; Bai, L.; Yang, J.; Yang, W. Emerging Flexible Thermally Conductive Films: Mechanism, Fabrication, Application. *Nano-Micro Lett.* **2022,** *14*, 127. https://doi.org/10.1007/s40820-022-00868-8 .
4. Hassan, T.; Salam, A.; Khan, A.; Khan, S.U.; Khanzada, H.; Wasim, M.; Khan, M.Q.; Kim, I.S. Functional nanocomposites and their potential applications: A review. *J. Polym. Res.* **2021,** *28*, 1-22. https://doi.org/10.1007/s10965-021-02408-1
5. Wang, X.; Zhang, M.; Zhang, L.; Xu, J.; Xiao, X.; Zhang, X. Inkjet-printed flexible sensors: From functional materials, manufacturing process, and applications perspective. *Mater. Today Commun.* **2022,** *31*, 103263. https://doi.org/10.1016/j.mtcomm.2022.103263 .
6. Li, C.; Yang, Y.; Xu, G.; Zhou, Y.; Jia, M.; Zhong, S.; Gao, Y.; Park, C.; Liu, Q.; Wang, Y.; Akram, S.; Zeng, X.; Li, Y.; Liang, F.; Cui, B.; Fang, J.; Tang, L.; Zeng, Y.; Hu, X.; Gao, J.; Mazzanti, G.; He, J.; Wang, J.; Fabini, D.; Teyssedre, G.; Cao, Y.; Wang, F.; Zi, Y. Insulating materials for realising carbon neutrality: Opportunities, remaining issues and challenges. *High Voltage* **2022,** 7, 610-632. https://doi.org/10.1049/hve2.12232
7. Khan, M.; Li, T.; Hayat, A.; Zada, A.; Ali, T.; Uddin, I.; Hayat, A.; Khan, M.; Ullah, A.; Hussain, A.; Zhao, T. Retracted: A Concise Review on the Elastomeric Behavior of Electroactive Polymer Materials. Int. J. Energy Res. **2021,** 45, 14306-14337. https://doi.org/10.1002/er.6747
8. Li, L.; Cheng, J.; Cheng, Y.; Han, T.; Liu, Y.; Zhou, Y.; Zhao, G.; Zhao, Y.; Xiong, C.; Dong, L.; Wang, Q. Significant Improvements in Dielectric Constant and Energy Density of Ferroelectric Polymer Nanocomposites Enabled by Ultralow Contents of Nanofillers. *Adv. Mater.* **2021**, *33*, 2102392. https://doi.org/10.1002/adma.202102392.
9. Cao, X.; Xiong, Y.; Sun, J.; Zhu, X.; Sun, Q.; Wang, Z.L. Piezoelectric Nanogenerators Derived Self-Powered Sensors for Multifunctional Applications and Artificial Intelligence. *Adv. Funct. Mater.* **2021,** *31*, 2102983. https://doi.org/10.1002/adfm.202102983.
10. Aziz, T.; Ullah, A.; Ali, A.; Shabeer, M.; Shah, M.N.; Haq, F.; Iqbal, M.; Ullah, R.; Khan, F.U. Manufactures of bio-degradable and bio-based polymers for bio-materials in the pharmaceutical field. *J. Appl. Polym. Sci.* **2022,** *139*, e52624. https://doi.org/10.1002/app.52624.
11. Sun, Q.J.; Lai, Q.T.; Tang, Z.; Tang, X.G.; Zhao, X.H.; Roy, V.A.L. Advanced Functional Composite Materials toward E-Skin for Health Monitoring and Artificial Intelligence. *Adv. Mater. Technol*. **2023,** *8*, 2201088. https://doi.org/10.1002/admt.202201088.
12. Miah, M.R.; Yang, M.; Hossain, M.M.; Khandaker, S.; Awual, M.R. Textile-based flexible and printable sensors for next generation uses and their contemporary challenges: A critical review. *Sens. Actuators A Phys.* **2022,** *344*, 113696. https://doi.org/10.1016/j.sna.2022.113696.
13. González, F.J.; González-Castillo, E.I.; Peña, A.; Belmontes, F.A. Nanofillers and Nanomaterials for Green Based Nanocomposites. In Green-Based Nanocomposite Materials and Applications; Springer International Publishing: Cham, **2023**; pp. 13-30. https://doi.org/10.1007/978-3-031-18428-4_2

14. Shameem, M.M.; Sasikanth, S.M.; Annamalai, R.; Raman, R.G. A brief review on polymer nanocomposites and its applications. Mater. Today Proc**. 2021,** 45, 2536-2539. https://doi.org/10.1016/j.matpr.2020.11.254
15. Alejandre, C.; Akizu-Gardoki, O.; Lizundia, E. Optimum operational lifespan of household appliances considering manufacturing and use stage improvements via life cycle assessment. Sustain. Prod. Consum. **2022,** 32, 52-65. https://doi.org/10.1016/j.spc.2022.04.007
16. Reiss, P.; Couderc, E.; De Girolamo, J.; Pron, A. Conjugated polymers/semiconductor nanocrystals H\hybrid materials—preparation, electrical transport properties and applications. *Nanoscale* **2011**, 3, 446-489. https://doi.org/10.1039/C0NR00403K.
17. Sinha, S.; Chatterjee, S.K.; Ghosh, J.; Meikap, A.K. Electrical transport properties of polyvinyl alcohol–selenium nanocomposite films at and above room temperature. *J. Mater. Sci.* **2015,** *50*, 1632-1645. https://doi.org/10.1007/s10853-014-8724-z.
18. Guchhait, P.K.; Bhandari, S.; Singh, S.; Rahaman, M. Study on the effect of nanosilica particles on morphology, thermo-mechanical and electrical properties of liquid polysulfide modified epoxy hybrid nanocomposites. *Int. J. Plast. Technol.* **2011,** *15*, 150-162. https://doi.org/10.1007/s12588-011-9017-x.
19. Mazumder, R.; Seal, A.; Sen, A.; Maiti, H.S. Effect of Boron Addition on the Dielectric Properties of Giant Dielectric $CaCu_3Ti_4O_{12}$. *Ferroelectrics* **2005,** *326*, 103-108. https://doi.org/10.1080/00150190500318644.
20. Amroun, M.N.; Khadraoui, M. AC conductivity and dielectric studies of $Cd_{0.8}Sn_{0.2}S$ thin films. *Int. J. Numer. Model.: Electron. Netw. Devices Fields* **2019,** *32*, e2617. https://doi.org/10.1002/jnm.2617.
21. Sreekala, P.S.; Honey, J.; Aanandan, C.K. Development and characterization of camphor sulphonic acid doped polyaniline film with broadband negative dielectric constant for microwave applications. *Mater. Res. Express* **2018,** *5*, 056302. https://doi.org/10.1088/2053-1591/aabe0f.
22. Prabakar, K.; Narayandass, S.K.; Mangalaraj, D. Dielectric and electric modulus properties of vacuum evaporated $Cd_{0.8}Zn_{0.2}Te$ thin films. *Mater. Sci. Eng. B* **2003,** *98*, 225-231. https://doi.org/10.1016/S0921-5107(03)00043-6.
23. Suman, C.K.; Prasad, K.; Choudhary, R.N.P. Complex impedance studies on tungsten-bronze electroceramic: $Pb_2Bi_3LaTi_5O_{18}$. *J. Mater. Sci*. **2006,** *41*, 369-375. https://doi.org/10.1007/s10853-005-2620-5.
24. Postnikov, V.S.; Pavlov, V.S.; Turkov, S.K. Internal friction in ferroelectrics due to interaction of domain boundaries and point defects. *J. Phys. Chem. Solids* **1970,** *31*, 1785-1791. https://doi.org/10.1016/0022-3697(70)90168-X.